Surface structures on sputtered/annealed WC(0001)

1999 J. Phys.: Condens. Matter 12 773

(http://iopscience.iop.org/0953-8984/12/6/302)

J. Phys.: Condens. Matter **11** (1999) 773–782. Printed in the UK PII: S0953-8984(99)08283-1

Surface structures on sputtered/annealed WC(0001)

M Göthelid and E Janin
Materialfysik, KTH, 10044 Stockholm, Sweden

Received 30 September 1999

Abstract. We use scanning tunnelling microscopy, Auger electron spectroscopy and low energy electron diffraction to study different tungsten and carbon terminated surface reconstructions on the sputtered/annealed WC(0001) surface. The tungsten terminated surface encompasses a $(\sqrt{7}\times\sqrt{7})$R19° W-trimer structure, a $(\sqrt{3}\times\sqrt{7})$ reconstruction representing a transition structure from the $(\sqrt{7}\times\sqrt{7})$R19° reconstruction to a (6×1) phase which consists of a quadratic W overlayer on the first close-packed carbidic carbon layer. The carbon terminated WC(0001) surface consists of a single graphitic carbon layer on top of the (6×1) structure.

1. Introduction

Transition metal carbides are attractive for hard coatings and tool manufacturing thanks to their hardness, high melting points and metallic conductivity [1]. They also exhibit interesting catalytic properties [2]. Tungsten carbide, for example, is used in hydrogen/oxygen recombination reactions in batteries [3]. These catalytic properties depend, of course, on the surface geometry and chemical composition.

Generally the close packed polar (111) surfaces of the NaCl structure transition metal carbides TiC, TaC, NbC, HfC and ZrC were believed to be non-reconstructively metal terminated on top of a full layer of carbon [4–13]. However, Bradshaw *et al* [6, 7] found from Auger and LEED measurements that the TiC(111) (1×1) surface contains both Ti terminated and C terminated domains. At higher carbon concentration a graphitic overlayer structure is formed [14]. STM images from this graphitic surface showed a periodic superlattice arising from the coincidence of the hexagonal graphite layer and the close packed TiC(111) substrate [14].

The $VC_{0.80}(111)$ surface presents an interesting exception within the NaCl structure transition metal carbides since it reconstructs in a metal terminated (8×1) structure together with a carbon terminated $(\sqrt{3}\times\sqrt{3})$R30° structure after sputtering and annealing above 900 °C [15]. At lower annealing temperatures (700–900 °C) a non-reconstructed meta-stable vanadium terminated (1×1) surface was obtained [16]. Surface shifted components in the C 1s core level were found on both $VC_{0.80}(111)$ (8×1) and (1×1) surfaces and the $VC_{0.8}(100)$ surface [17] indicating a mixed termination of all these surfaces in agreement with the STM findings [15].

The (8×1) structure consists of a square vanadium layer on top of a hexagonal substrate as proposed from a scanning tunnelling microscopy (STM) experiment on this surface [15]. STM images from the (8×1) structure suggested a buckling of the top layer, an effect of the different bond sites with respect to the underlying close packed substrate [15]. An impact collision ion scattering spectrometry (ICISS) study verified the square overlayer but questioned

0953-8984/99/060773+10$19.50

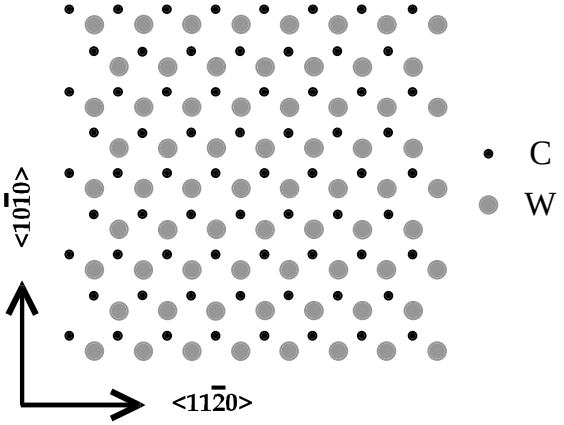

Figure 1. Top view drawing of the hcp WC(0001) surface with large grey circles for W and small black circles for C.

the buckling [18]. Their results instead hinted at a perfectly planar vanadium layer residing on a close packed carbon layer. The corrugation observed in the STM images was suggested to be an electronic effect [18].

WC crystallizes in the hcp structure. A top view illustration of this structure is shown in figure 1, with orthogonal crystal directions indicated by arrows. The in-plane lattice parameter is 2.91 Å. The first study on a single crystal WC(0001) surface was reported in 1984 by Stefan *et al* [19], who used angle resolved photoelectron spectroscopy (ARPES) and Auger electron spectroscopy (AES). Later a core level photoemission study on this surface revealed surface-shifted components both in the W 4f and the C 1s levels [20]. These surface shifts were interpreted as resulting from carbon and tungsten terminated areas on the surface similar to the VC surfaces. The interaction of various molecules: O_2 [21], CO and NO [22] with the clean WC(0001) surface was recently investigated by Brillo *et al*. The surface was assumed to be non-reconstructed, as one may expect from the (1×1) low energy electron diffraction (LEED) pattern, with co-existing carbon and tungsten terminated surface regions [21, 22]. However, no details of the surface geometry were discussed and no other LEED patterns were reported.

The surface structures on the clean WC(0001) are not well understood and the influence of the chemical composition at the surface has not been explored up to now. We have therefore studied the surface structures appearing on sputter and annealing cleaned WC(0001) using scanning tunnelling microscopy, Auger electron spectroscopy and low energy electron diffraction.

2. Experimental details

The STM experiments were performed with a commercial Omicron ultra-high vacuum (UHV) STM using tungsten tips electro-chemically etched in an NaOH solution. The tips were cleaned *in situ* by Ar^+ ion sputtering. All images were recorded in constant current mode. Connected to the STM chamber is a preparation chamber comprising low energy electron diffraction (LEED), direct sample heating and Ar^+ ion sputtering. The AES experiments were performed in a separate UHV chamber utilizing a Perkin–Elmer cylindrical mirror analyser (CMA) with an integrated electron gun. The base pressure in all chambers was better than 1×10^{-10} Torr.

The sample was cut from a WC crystal grown at Sandvik-Coromant, Stockholm, Sweden. Samples from the same crystal have previously been used for Auger electron spectroscopy (AES) and photoemission studies [19, 20]. Cleaning of the WC(0001) sample was achieved by direct heating at 1700 °C or by Ar^+ ion sputtering at 500 eV and subsequent annealing at

$\sim$1200 °C. The pressure was kept below 1×10^{-9} Torr during annealing. The temperature was measured with a pyrometer.

The surface composition could be changed: graphitic carbon could be removed by annealing the sample at 800 °C in oxygen atmosphere ($P \sim 1 \times 10^{-6}$ Torr), while carbon could be added to a carbon deficient surface by annealing in C_2H_4 ($P \sim 1 \times 10^{-6}$ Torr). Prolonged sputtering and subsequent annealing also resulted in a graphite-like surface.

Figure 2 shows an Auger spectrum displaying the relevant Auger lines in this study in the kinetic energy range from 100 to 300 eV. The peak-to-peak intensity ratio ($\sim$1) of the W_{NOO} and C_{KLL} lines (given by the horizontal bars in the figure) and the line profile indicates, after comparison with data found in the literature [21, 22], that the spectrum corresponds to the graphitic WC(0001) surface. The LEED pattern from this surface was (1×1) with additional streaks between the integer order spots, which did not appear until after several hours of cooling down due to the high temperature treatment.

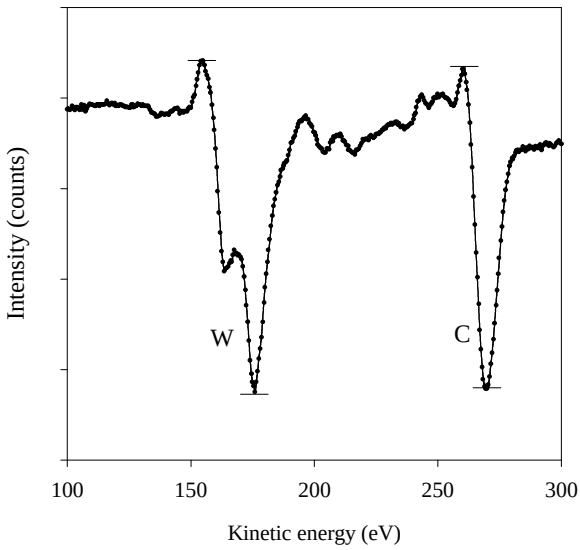

Figure 2. Auger spectrum from the graphitic WC(0001) surface.

On the tungsten rich surfaces sharp and clear (6×1) and $(\sqrt{7} \times \sqrt{7})$R19° LEED patterns were observed also only after several hours of cooling down while directly after heating (1×1) patterns with weak additional streaks were observed. The dominating tungsten terminated surface reconstruction is the (6×1) structure with an Auger peak-to-peak W/C ratio around 2.

We estimate the graphitic layer to be one monolayer thick by calculating the expected intensity ratios from the two surface structures, using an exponential attenuation model neglecting diffraction effects. We assume that the (6×1) structure (or a structure with a similar surface stochiometry) remains under the graphitic layer (this assumption is discussed and validated later in this paper).

3. Results and discussion

3.1. Graphitic WC(0001)

Figure 3(a) is a 500×1000 Å^2 overview empty state STM image from the graphitic WC(0001) surface from which the Auger spectrum shown in figure 2 above was recorded. The surface consists of large flat terraces occasionally interrupted by islands as seen in the figure. These

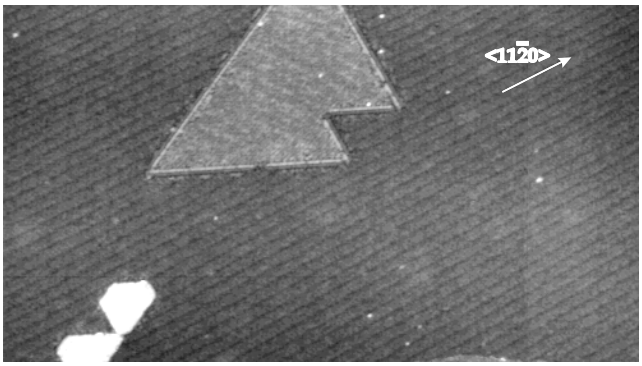

(a)

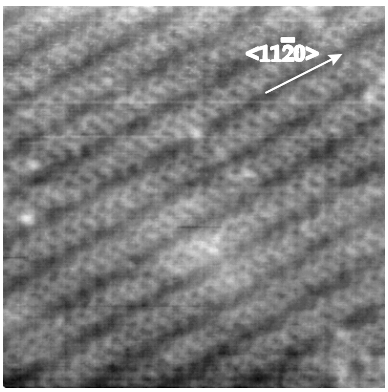

(b)

Figure 3. Empty state (+1 V, 1 nA) STM images from the graphitic WC(0001) surface: (a) is a 500×1000 Å^2 overview and (b) is a 200×200 Å^2 close up image.

islands appear in a low concentration over the surface, less than 5%. The dominating structure is the structure seen on the surrounding terrace with approximately 15 Å wide bands running in $\langle 11\bar{2}0 \rangle$ directions, as determined from their parallelity to step edges. The width of the bands is the same as for the (6×1) structure, which we will discuss later. The corrugation across the rows is 0.15 Å.

A high resolution (200×200 Å^2) empty state STM image in figure 3(b) reveals a honeycomb pattern superposed on the wider row structure in agreement with a graphite structure. A drawing of a graphite layer is shown in figure 4. The distance between the centre of the hexagons is 2.46 Å, while the distance between the unit cells measured in the STM image is around 4.2 Å, which corresponds nicely to a $\sqrt{3}$ graphite distance. Hence, the STM image probes only three out of six carbon atoms in the graphite lattice. This has previously been observed on graphite covered Pt(111) [23] and Pt(110) [24] surfaces and near defects or contaminations on the HOPG surface [25]. The in-equivalency of the two carbon atoms on HOPG can be understood from the geometrical difference with respect to the second carbon layer. However, in the case of graphite on the Pt surface two unique carbon environments could not easily be singled out [23, 24], and the preferential imaging of every second carbon atom is most probably an effect within the graphite layer itself induced by the presence of the substrate.

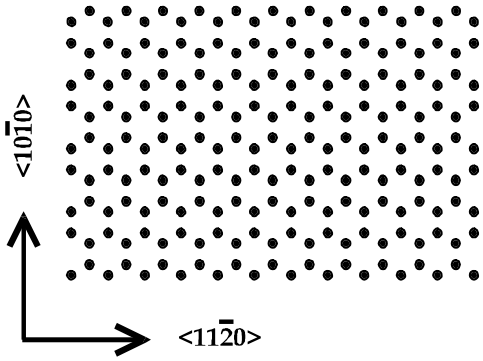

Figure 4. A top view drawing of a single layer of graphite.

The moiré superstructure has a twofold symmetry along the $\langle 11\bar{2}0\rangle$ direction, implying a preferred orientation with the graphite layer $\langle 11\bar{2}0\rangle$ direction aligned with the substrate $\langle 11\bar{2}0\rangle$ axis. The superstructure observed here cannot be expected from a threefold symmetric overlayer on a threefold substrate, as previously observed on the graphitic TiC(111) surface [14] and on the graphite covered Pt(111) [23]. On the Pt(111) surface several different moiré patterns were observed due to different orientations of the carbon overlayer with respect to the close packed Pt(111) substrate [23]. Hence the unique orientation observed on the WC(0001) surface must reflect the symmetry of the first layer below the graphitic layer.

Unfortunately with STM the layers beneath the top layer are only accessible in exceptional cases. The tunnelling voltage and current did not show any strong influence on the rows or the hexagonal structure as recently reported for the Pt(110)–C surface where for some tunnelling conditions the overlayer became 'transparent' and allowed a detailed explanation of the substrate below the graphite [24]. However, a possible solution can be found from the tungsten rich (6×1) structure described below.

3.2. Tungsten terminated WC(0001) structures

Two filled and empty state (200×200) Å^2 STM images recorded from the (6×1) surface are shown in figure 5. The reconstruction consists of $\sim$15 Å broad bands running along the

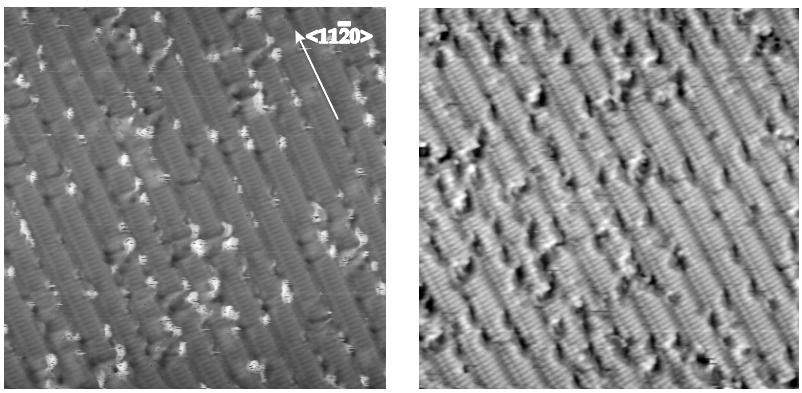

(a) (b)

Figure 5. 200×200 Å^2 STM images from the tungsten rich WC(0001) (6×1) surface recorded at sample biases -1 and +1 V respectively and tunnelling current 1 nA.

$\langle 11\bar{2}0\rangle$ directions of the crystal, similar to the graphitic surface. The distance between the protrusions within the rows is 2.9 Å, i.e. a WC(0001) in-plane distance. In the perpendicular direction no atomic resolution is observed at this scale. The corrugation on top of the rows is 0.27 Å and 0.42 Å across the rows. Thus, comparison of the STM images reveals that the (6×1) reconstruction remains under the graphitic top layer as indicated above.

The high resolution (40×40 Å^2, 5 nA, 0.1 V) STM image in figure 6(a) partly resolves a quadratic overlayer, very similar to the vanadium terminated (8×1) reconstruction on the $VC_{0.8}(111)$ surface [15–18]. In figure 6(b)–(d) we propose, based on the models from [15], three possible atomic models to form the (6×1) surface reconstruction. The basic idea is a quadratic tungsten overlayer on top of the carbon terminated substrate. In the model large grey circles represent tungsten atoms in the top layer and the small black dots represent carbon atoms in the first hexagonal layer. The tungsten coverage is 5/6 monolayer (ML) in the top layer, where 1 ML is defined by the number of atoms in the ideal bulk terminated WC(0001) surface. The (6×1) unit cell is indicated in the model. The tungsten–tungsten distance along the $\langle 11\bar{2}0\rangle$ direction is the same as the WC(0001) in plane distance while in the perpendicular direction five 'quadratic' W–W distances correspond to a $3\sqrt{3}$ substrate distance.

The three different models are formed by putting a row of tungsten atom on a top site (b), on a bridge site (c) or on a hollow site (d). In the top site model one W atomic row is fixed in the top site and the four remaining rows are in 'near hollows' (NH in the figure) slightly shifted towards the top site or the bridge site. The bridge model on the other hand has one row of W atoms in the bridge site and two out of five rows in 'near top' (NT in the figure) while two rows are in 'near hollow'. Finally, the hollow model is very similar to the bridge model but with one row of atoms in the hollow site, one row in 'near hollow', two rows in 'near top'

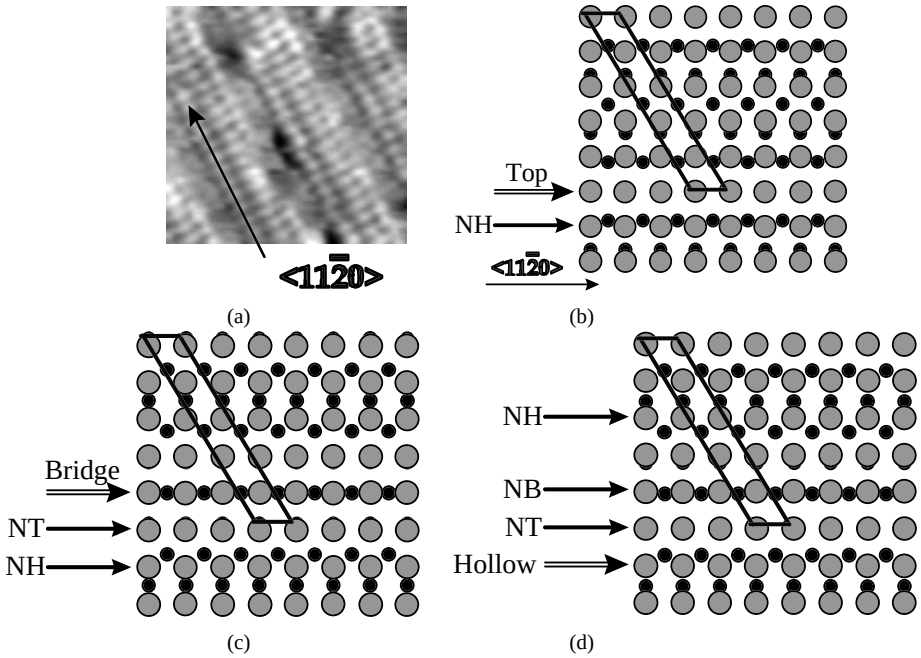

Figure 6. High resolution empty state image (5 nA, 0.1 V, 40×40 Å^2) in which a quadratic overlayer is resolved. (b)–(d) are structural models proposed for this surface reconstruction. The black circles represent carbon atoms and the grey circles represent tungsten atoms.

and finally one row in 'near bridge' (NB in the figure). To determine the 'correct' model from the STM images alone is not decisive, especially with the close similarity between the bridge and hollow models.

Close packed overlayers, on non-hexagonal surfaces, have been observed on Pt(100) and PtNi(100) [26] and can be explained by the lower surface energy of a close packed surface layer. Quadratic overlayers on hexagonal surfaces are less common. However, as mentioned above, a quadratic vanadium overlayer was previously observed on the $VC_{0.80}(111)$ surface. The (8×1) periodicity observed in that case was explained by a coincidence of a 7/8 monolayer (ML) dense quadratic V layer with the hexagonal $VC_{0.80}(111)$ substrate [15].

A qualitative explanation for the quadratic V layer was put forward based on simple band filling, structural stability and cohesive energy of various carbides in the 3d and 4d series [15, 27]. A maximum in cohesive energy was obtained for TiC in the 3d, NbC in the 4d and TaC in the 5d series respectively, as shown by the plot of the cohesive energies for 3d, 4d and 5d carbides in figure 7. When plotted against the number of electrons (e^-) per atom this maximum was between 4 and 4.5 e^-/atom [27]. It was argued that carbides on the up-hill side of the maximum would gain stability by increasing the number of valence electrons while for compounds on the down-hill side it would be favourable to lower the valence electron density, thus decreasing the number of atoms at the surface. The maximum at TaC along with the arguments in [15] suggests that WC would gain stability by lowering the surface density of atoms. From the different crystal structure of WC one may argue that this reasoning is not valid. However, the (111) surfaces of the NaCl carbides present alternating metal and carbon layers similar to the WC(0001) structure. Furthermore, the crystal structure was not explicitly taken into account in the calculations [27].

The $(\sqrt{7} \times \sqrt{7})R19^\circ$ reconstruction was found at lower tungsten concentrations than the (6×1) structure. An empty state (0.7 V, 1 nA) 200×200 Å^2 STM image from this reconstruction is presented in figure 8(a). A relatively large number of defects in the form of missing atoms is seen. This is a general remark valid for all the tungsten rich structures on this surface; they all have a high defect density. A closer look at the surface in figure 8(b) (60×60 Å^2) reveals the triangular shape of the small building block. The distance between

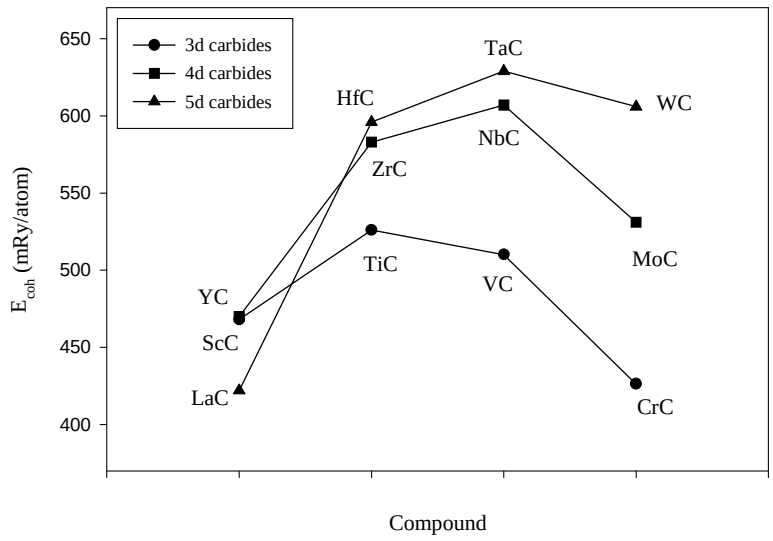

Figure 7. The cohesive energies for the 3d, 4d and 5d carbides, plotted from results in [27].

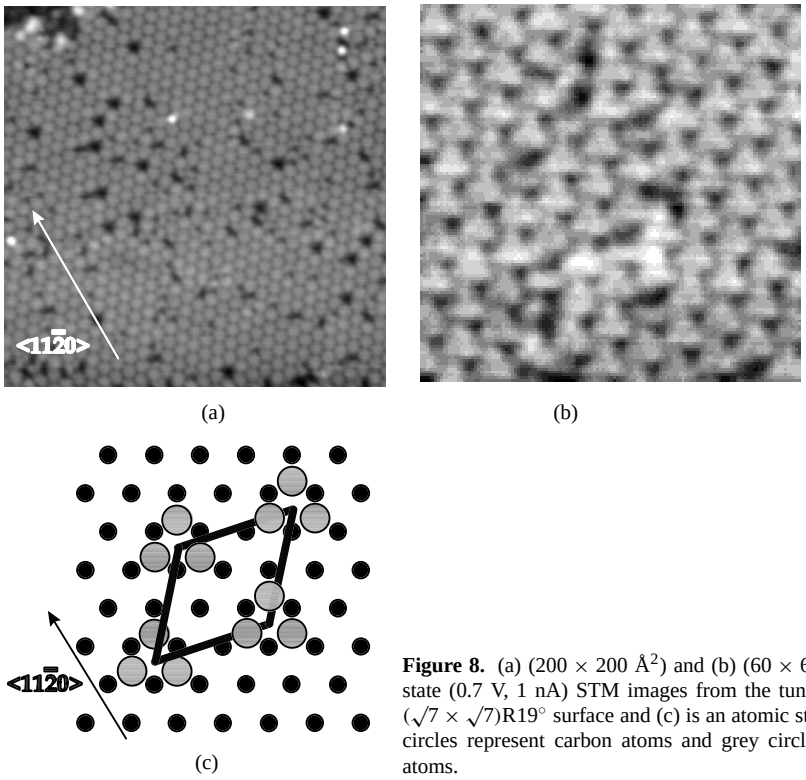

Figure 8. (a) (200×200 Å^2) and (b) (60×60 Å^2) are two empty state (0.7 V, 1 nA) STM images from the tungsten rich WC(0001) ($\sqrt{7} \times \sqrt{7}$)R19° surface and (c) is an atomic structure model. Black circles represent carbon atoms and grey circles represent tungsten atoms.

the protrusions within the triangles is, within the accuracy of such a measurement, an in-plane WC(0001) bulk distance, i.e. 2.9 Å. The corrugation in the image is 0.15 Å.

We propose that the triangularly shaped features reflect three tungsten atoms as presented in the model in figure 8(c). The W atoms are placed in hollow sites with respect to the first layer carbon atoms since this is the expected position in the WC bulk crystal. The tungsten coverage in the top layer of the model is 3/7 ML, which is lower than the 5/6 ML proposed for the (6×1) reconstruction, in agreement with the respective Auger intensities.

In areas between the (6×1) and $(\sqrt{7} \times \sqrt{7})$ structures smaller ordered regions were found. An empty state 200×200 Å^2 image from one such area is presented in figure 9(a). The surface has a high density of defects and kinks which gives very small coherent domains of this surface structure and this was not observed in LEED. Furthermore, the reconstructed regions were rather small (∼500 Å).

A 30×30 Å^2 high resolution empty state STM image is presented in figure 9(b). The image has been rotated. The unit cell has a rhombic shape with one side having a $\sqrt{3}$ length and the other side a $\sqrt{7}$ length. One bright protrusion dominates the unit cell. A more shallow and broad structure is observed between the high bumps. The height difference is 0.08 Å between the higher and lower structures, and 0.42 Å between the bright protrusion and the valleys between the rows. Assuming that the height difference between the white and the grey protrusions reflects a difference in adsorption site of the top layer tungsten atoms there are at least two different sites for W in this structure. Since the (6×1) structure includes several sites and the $(\sqrt{7} \times \sqrt{7})$ only comprises the hollow site the $(\sqrt{3} \times \sqrt{7})$ structure thus may represent a transition phase from the (6×1) to the $(\sqrt{7} \times \sqrt{7})$ phases, for coverages between 3/7 ML in the $(\sqrt{7} \times \sqrt{7})$ reconstruction and 5/6 ML in the (6×1).

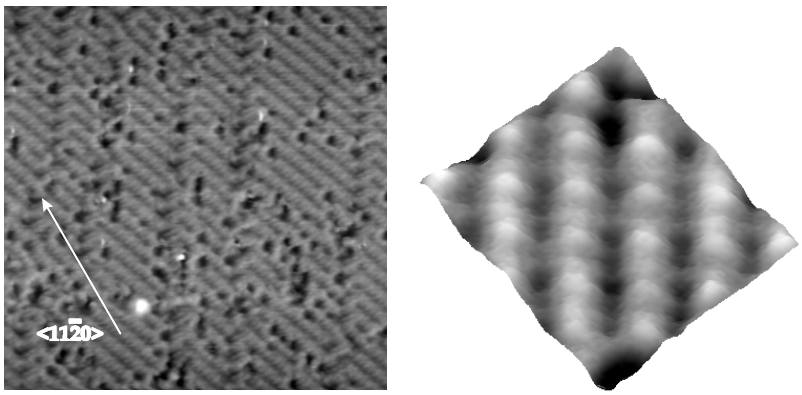

(a) (b)

Figure 9. A 200 × 200 Å^2 overview STM image from the ($\sqrt{3} \times \sqrt{7}$) surface structure (a) and a high resolution (30 × 30 Å^2) STM image (b). The black circles represent carbon atoms and the grey circles represent tungsten atoms.

4. Conclusions

We have used Auger electron spectroscopy, low energy electron diffraction and scanning tunnelling microscopy to study surface structures on the sputter–annealing cleaned WC(0001) surface. In particular we have found a tungsten terminated (6 × 1) reconstruction consisting of a square net of tungsten atoms on top of a hexagonal carbon layer, with a 5/6 ML tungsten surface coverage. At lower tungsten coverage a ($\sqrt{7} \times \sqrt{7}$)R19° phase was found in which the surface tungsten atoms occupy hollow sites. A transition structure intermediate to these two structures was also observed. Finally, a graphitic surface structure was found, determined to be a single layer of graphitic carbon on top of the (6 × 1) phase. The reconstruction diagram thus appears more complicated than hitherto believed.

Acknowledgments

This project was financially supported by the Swedish Natural Science Council (NFR) and the K&A Wallenberg Foundation. We thank Dr Rundgren J for fruitful discussions.

References

[1] Toth L E 1971 *Transition Metal Carbides and Nitrides* (New York: Academic)
[2] Oyama S T 1992 *Catal. Today* **15** 179
[3] Diets H, Dittmar L, Ohms D, Radwan M and Weisener K 1992 *J. Power Source* **40** 175
Nikolov I, Papzov G and Nadjenov V 1992 *J. Power Source* **40** 333
[4] Aono M, Oshima C, Zaima S, Otani S and Ishizawa Y 1981 *Japan. J. Appl. Phys.* **20** L829
[5] Zaima S, Shibata Y, Oshima C, Otani S, Aono M and Ishizawa Y 1985 *Surf. Sci.* **157** 380
[6] Bradshaw A M, van der Veen J F, Himpsel F J and Eastman D E 1980 *Solid State Commun.* **37** 37
[7] Weaver J H, Bradshaw A M, van der Veen J F, Himpsel F J, Eastman D E and Politis C 1980 *Phys. Rev.* B **22** 4921
[8] Souda R, Oshima C, Otani S, Ishizawa Y and Aono M 1988 *Surf. Sci.* **199** 154
[9] Kojima I, Orita M, Mizayaki E and Otani S 1985 *Surf. Sci.* **160** 153
[10] Edamoto K, Anazawa T, Shiobara E, Hatta M, Miyazaki E, Kato H and Otani S 1991 *Phys. Rev.* B **43** 3871
[11] Hayami W, Souda R, Aizawa T, Otani S and Ishizawa Y 1992 *Surf. Sci.* **276** 299

[12] Hulbert S L, Kato C C, Garrett R F, Bartynsky R A, Yang S, Weinert M and Jensen E 1991 *J. Vac. Sci. Technol.* A **9** 1919
[13] Hwang H *et al* 1992 *Surf. Sci.* **271** 299
[14] Itoh H, Ichinose T, Oshima C, Ichinokawa T and Aizawa T 1991 *Surf. Sci.* **254** L437
[15] Hammar M, Törnevik C, Rundgren J, Gauthier Y, Flodström S A, Håkansson K L, Johansson L I and Häglund J 1992 *Phys. Rev.* B **45** 6118
[16] Rundgren J, Gauthier Y, Baudoing-Savois R, Joly Y and Johansson L I 1992 *Phys. Rev.* B **45** 4445
[17] Håkansson K L, Johansson L I, Hammar M and Göthelid M 1993 *Phys. Rev.* B **47** 10 769
[18] Hammar M, Steel B E and Tsong I S T 1994 *Nucl. Instrum. Methods Phys. Res.* B **85** 429
[19] Stefan P M, Shek M L, Lindau I, Spicer W E, Johansson L I, Herman F, Kasowski R V and Brogren G 1984 *Phys. Rev.* B **29** 5423
[20] Håkansson K L, Johansson H I P and Johansson L I 1994 *Phys. Rev.* B **49** 2035
[21] Brillo J, Kuhlenbeck H and Freund H J 1998 *Surf. Sci.* **409** 199
[22] Brillo J, Sur R, Kuhlenbeck H and Freund H J 1998 *Surf. Sci.* **397** 137
[23] Land T A, Michely T, Behm R J, Hemminger J C and Comsa G 1992 *Surf. Sci.* **264** 261
[24] Janin E, Göthelid M and Karlsson U O *Appl. Surf. Sci.* at press
[25] See e.g. Park Sang-Il and Quate C F 1986 *Appl. Phys. Lett.* **48** 11
Kubawara M, Clarke D R and Smith D A 1990 *Appl. Phys. Lett.* **56** 2396
Binnig G, Fuchs H, Gerber Ch, Rohrer H, Stoll E and Tosatti E 1986 *Europhys. Lett.* **1** 31
[26] Borg A, Hilmen A M and Bergene E 1994 *Surf. Sci.* **306** 10
Gauthier Y, Baudoing-Savois R, Rundgren J, Hammar M and Göthelid M 1995 *Surf. Sci.* **327** 100
[27] Häglund J, Grimvall G, Jarlborg T and Fernandez-Guillermet A 1991 *Phys. Rev.* B **43** 14 400
Fernandez-Guillermet A, Häglund J and Grimvall G 1992 *Phys. Rev.* B **45** 11 557
Fernandez-Guillermet A, Häglund J and Grimvall G 1993 *Phys. Rev.* B **48** 11 673